PERGAMON

International Journal of Heat and Mass Transfer 45 (2002) 4191–4200

International Journal of HEAT and MASS TRANSFER

www.elsevier.com/locate/ijhmt

Heat transfer to a row of impinging jets in consideration of optimization

P. Brevet [a], C. Dejeu [b,1], E. Dorignac [a], M. Jolly [a], J.J. Vullierme [a,*]

[a] *Laboratoire d'Etudes Thermiques (UMR CNRS 6608), ENSMA, 1 Avenue Clément Ader, BP 40109, 86961 Futuroscope Chasseneuil Cedex, France*

[b] *SNECMA Moteurs, Department of Turbines, Site de Villaroche, Reau, 77550 Moissy Cramayel, France*

Received 23 July 2001; received in revised form 1 January 2002

Abstract

In the current study the heated-thin-foil technique is used jointly with infrared thermography to evaluate accurately the heat transfer characteristics of one row of jets impinging on a flat plate. The impingement is confined by the test section and spent air is constrained to exit in only one direction. The configuration and parameters variation range are similar to those encountered in turbine internal cooling systems. The results are analysed in terms of local and averaged Nusselt number keeping in mind the design engineer preoccupation of minimizing the amount of cooling air taken from the compressor. The influence of the impingement distance Z/d, injection Reynolds number Re and spanwise spacing p/d between two holes of the row is presented. An optimum impingement distance is pointed out and some qualitative design rules for the two other parameters are underlined.

1. Introduction

The specific thrust and the thrust specific fuel consumption (TSFC) are the two important performance parameters of a turbojet or a turbofan. These two parameters are directly linked to two important variables which have to be set when designing such kind of advanced engines: the turbine inlet temperature (TIT) and the compressor pressure ratio. The specific thrust increases when the inlet temperature increases: the higher TIT is, the smaller and the lighter the engines can be kept. At a fixed TIT, a high compressor pressure ratio will globally reduce the TSFC. That is why it is generally desirable to increase the TIT and the compressor pressure ratio. However, as TIT is increased, the amount of heat transferred to the turbine blades is increased as well. Furthermore, as the compressor pressure ratio is increased, the total temperature of the available cooling air is increased as well. Turbine materials should thus withstand higher and higher heat flux coming from the hot combustion gas thanks to blade internal cooling systems and film cooling systems which use themselves hotter and hotter cooling air extracted from the last stages of the compressor. Hence the turbine cooling problems are intensified and become nowadays more and more challenging. Not only a precise thermal analysis and detailed characterization of the convective boundary conditions on external and internal blade surfaces are required so that the engineer is able to predict component temperatures field and life expectancy accurately but it becomes all the more important to optimize the cooling methods chosen and the blade geometry to minimize the engine loss of efficiency due to the extraction of cooling air from the compressor.

Jet impingement is one of the most efficient solutions for internal cooling in so far as it produces very large forced-convection heat transfer rates. It is widely used on the vane inner surfaces of modern gas turbines to prevent the metal temperature from overheating. It is especially introduced where the thermal conditions are the most severe: the nozzle guide vane, the leading edge

* Corresponding author. Tel.: +33-5-4949-8134; fax: +33-5-4949-8101.

E-mail addresses: clement.dejeu@snecma.fr (C. Dejeu), vullierme@let.ensma.fr (J.J. Vullierme).

[1] Tel.: +33-1-6059-7123

0017-9310/02/$ - see front matter
PII: S0017-9310(02)00128-X

Nomenclature

c	chordwise spacing between two rows, m
d	impingement jet hole diameter, m ($d = 10$ mm)
e	thickness of the impingement plate, m
E	thickness of the injection plate, m ($E/d = 1$)
G_s	mass flow rate of coolant per unit area of cooled surface, kg/m^2 s
h	heat transfer coefficient, W/m^2 K
k	thermal conductivity, W/m K
Nu	Nusselt number, $Nu = hd/k_{air}$
p	spanwise spacing between two holes of the same row, m
q	heat flux density, W/m^2
Re	injection Reynolds number, $Re = V_j d/v$
T	temperature, K
V	velocity, m/s
x	streamwise (chordwise) distance measured from the center of the most upstream jets row, m
y	spanwise distance centered on middle of the jets row, m
Z	jet-to-plate spacing, m

Greek symbols

ε	emissivity
v	kinematic viscosity, m^2/s
ρ	density, kg/m^3
σ	Stefan-Boltzmann constant (5.67×10^{-8} W/m^2 K^4)

Subscripts

air	relative to air
amb	relative to the ambient air
aw	adiabatic wall
b	impingement plate back side
c	relative to convection
j	impingement jet
f	impingement plate front side
inj	injection wall
r	relative to radiation
w	impingement wall

and midspan regions of the vanes. Son et al. [1] underline finally that the impingement technique is more robust than the film cooling technique which is prone to external deposition. Furthermore, heat transfer uniformity can be achieved more easily with jet impingement compared to multi-pass systems or serpentine passages equipped with ribs, pin fins, or roughness elements, for which the cooling potential is decreasing along the passage.

2. Previous studies

Many experimental and numerical investigations on heat transfer and flow characteristics of impinging jets have been carried out and are still conducted. Martin [2], Downs and James [3], Jambunathan et al. [4] and Viskanta [5] referred to a large panel of fundamental studies and presented complete reviews on the main parameters influence on heat transfer. Behbahani and Goldstein [6] used the liquid crystal technique to evaluate heat transfer for a staggered arrays of jets impinging on a flat surface and gave qualitative results relatively to the jet-to-impingement plate distance. Local profiles and spanwise-averaged heat transfer for three staggered arrays of impinging air jets coefficients were reported by Hollworth and Cole [7]. They extracted from their measurements a few design rules to optimize such cooling systems. Van Treuren et al. [8,9] introduced a transient method to measure the heat transfer coefficient distribution over the complete surface of a plate impinged by inline and staggered arrays of jets. They pointed out a mechanism which thermally couples the injection plate temperature to the impingement plate temperature. It can notably influence the adiabatic wall temperature and hence the local heat transfer. This coupling phenomenon is probably to be linked to the fountain effect visualized by Saripalli [10] between two adjacent jets of a multi-jets. Son et al. [1] investigated the heat transfer and wall flow characteristics of an existing turbine impingement system. A staggered pattern was used and jet hole diameters were bigger downstream than upstream. Parsons and Han [11] looked at the effect of rotation on jet impingement heat transfer. Rotation alters the internal cooling air flow and these authors found that impingement heat transfer decreased up to 15–20% with rotation. Florschuetz et al. [12–16] conducted an extensive study for different arrays of jets. These authors extracted heat transfer correlations from their measurements. These correlations are nowadays widely used in the industry design process.

Impinging jets are thus a very attractive solution for blade cooling. One, two or three rows of impinging jets (arrays of jets) with a trailing edge discharge are especially used to cool the upper and under surfaces of the leading edge of the low-pressure stage vanes. Fig. 1 shows the kind of geometry which can be encountered in such a case.

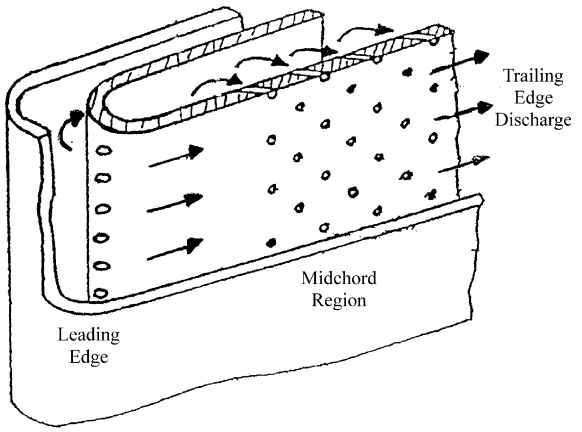

Fig. 1. Sketch of a low-pressure turbine vane internal cooling system based on jet impingement.

Impinging jets are typically generated with a thin perforated plate inserted into the vane and pressurized with air. Air is injected through the perforations and impinges on the vane inner surface. The curvature of the vane in this area is generally low enough to consider that impingement on a flat surface is appropriate to model this region. Then one can consider the impingement system as a channel formed by two parallel plates: the injection plate and the impinged plate. The air is constrained to evacuate in a single preferential direction toward the trailing edge.

The aim of the current work is to analyse accurately heat transfer generated by the impingement of one row of jets from the optimization point of view in such a configuration. The jets are confined and the parameters vary within ranges encountered in blade geometries. Detailed local heat transfer measurements lead to averaged Nusselt numbers which characterize the overall cooling efficiency. This efficiency is expressed for each set of parameters as a function of the total amount of cooling air used. This corresponds to one of the main preoccupations of the cooling system designer which is indeed to cool a given surface as efficiently as possible: one should obtain the maximum internal heat transfer using the minimum amount of coolant. The study investigates the influence of the injection Reynolds number Re. Five values are tested from 3000 to 20 000 (jet velocity from 4.5 to 30 ms^{-1}). The influence of the impingement distance Z/d ($Z/d = 1$, 2, 5 or 10) and the spacing p/d between two holes of the row ($p/d = 2$, 4, 6, 10) are evaluated as well. The temperature uniformity is not taken as an optimization criteria since our study is only concerned with the convective aspects of the problem and does not analyse conduction into the turbine walls. The injection Mach number is low enough ($M < 0.1$) so that no compressible effect is considered as it was shown in a previous study (Brevet et al. [17]).

3. Experimental setup and measurement technique

The experimental set-up is sketched in Fig. 2. It consists basically of a test section connected to a fan. One of the wall of the test section is equipped with injection holes connecting the test section to the ambient environment. This wall is called the injection plate. The fan creates a depression within the test section and pumps the air through the injection holes which generates the impinging jets. Total mass flow rate (sum of the mass flow rates in all the injection holes) is controlled and measured with a series of three parallely connected standard flowmeters (Fischer and Porter). The mass flow rate uniformity within the row of jets was verified for each impingement configuration thanks to previously calibrated pressure taps in each injection holes. The mass flow rate scattering among the injection holes is less than 4% when compared to the mean value obtained with the global flowmeters measurement. Velocity scattering is then less than 2%. The mass flow rate scattering is all the more negligible as Z/d is high. Finally it is acceptable to consider a single value of injection Reynolds number (based on the jet diameter) for all jets within the test range whatever the impingement configuration is. This value is known from the total impingement jet mass flow rate and the total jet open area.

The test section is rectangular and made of altuglass except for the impingement plate. Its spanwise dimension (y-direction) is 30d. The height of the test section is equal to the impinging distance and can be varied from 1d to 10d. The test section is closed at one of its end (the upstream side) whereas the other side (the downstream side) is connected to the flowmeters and the depressor. The test section length (streamwise, x-direction) is 95.5d. There are seven jets distributed in the spanwise direction (spacing p/d between two holes). They constitute a row of jets which is positioned 24d downstream from the closed side of the test section (one-row configuration).

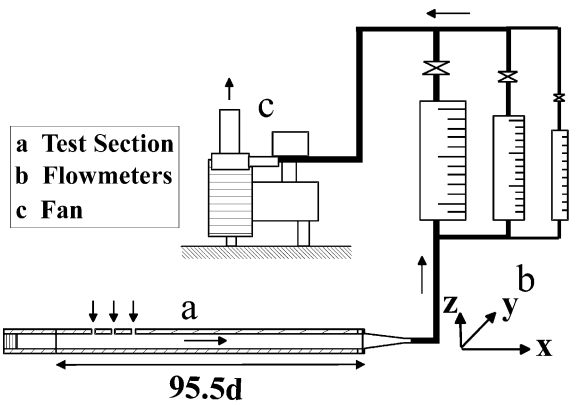

Fig. 2. Test rig.

Circular sharp-edged holes are used to generate the impinging jets. Their diameter d is equal to 10 mm and the injection plate thickness to jet diameter ratio E/d is equal to 1. Two extra rows of seven jets can eventually be added downstream of the first row to represent an array of inline jets as it can be found in turbine geometries (three-rows configuration). The streamwise spacing c/d between two rows is then equal to 10. These two rows are generally not used except to evaluate their influence on heat transfer generated by the first row. Since the injected air is sucked from the ambient environment around the test section and since the flow velocities involved in the experiment are low enough to neglect any recovery effect, the jet temperature T_j is equal to T_{amb}. The test section with the main geometric and flow parameters are sketched in Fig. 3.

The impingement plate is made of epoxy resin ($e = 1.6$ mm thick) whose thermal conductivity was measured with the laboratory facilities ($k_w = 0.32 \pm 2\%$ W/m K). Fifteen individual electric copper circuits (17.5 μm thick, 1.125 mm width) are printed on the impingement side (front side) of the plate. They are distributed in the streamwise direction and heat the plate by Joule effect. They were designed not to privilege any particular direction. Potentiometers are used to individually set the electric intensity injected in each circuit. The variation of resistivity with temperature is taken into account globally for a given circuit during the test run. A uniform heat flux density can thus be experimentally prescribed as a boundary condition on the entire front surface of the impingement plate. This uniformity has been verified before any test was run and is included within ±5% of the mean heat flux density over all the electric circuits. Yet the data post-processing takes into account the exact density heat flux of each circuit since small variations from a circuit to another may still exist. The surface temperature distribution T_b of the impingement plate back side is measured using an infrared camera (AGEMA Thermovision 880 SWB, image acquisition frequency: 25 Hz) (camera position 1—Fig. 4). This side of the plate is painted in black to give the surface the high and uniform emissivity required by infrared camera measurements. This emissivity was experimentally calibrated ($\varepsilon_b = \varepsilon_f = 0.96 \pm 0.02$). The

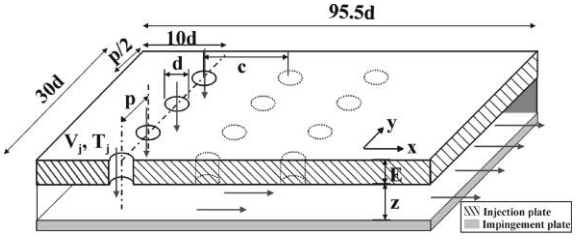

Fig. 3. Impingement parameters.

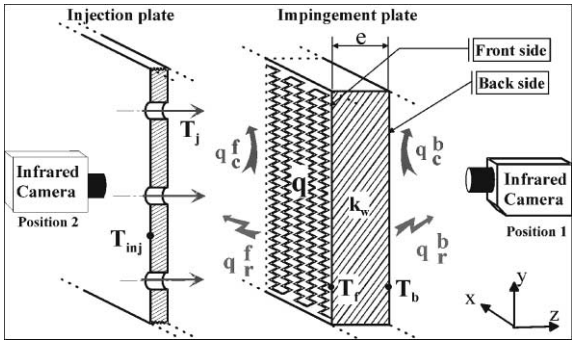

Fig. 4. Heat transfer measurement facilities and heat flux balance parameters.

spatial resolution is in the order of 0.6 mm (0.06d). The injection plate temperature T_{inj} is measured with the infrared camera as well ($\varepsilon_{inj} = 0.94 \pm 0.02$) (camera position 2—Fig. 4). This measurement is not influenced by the impingement plate radiation since altuglass is opaque to infrared radiation. T_{inj} is experimentally uniform all over the injection plate. Since both of its sides are submitted to temperatures very close to the ambient temperature, T_{inj} is close to T_{amb} and the injection plate temperature can be considered uniform across the plate thickness as well. Radiation from the impingement plate is nevertheless taken into account in the data postprocessing. Any infrared measurement is carried out over a time period of 10 s and then time-averaged to improve the thermal precision. Air temperature is measured with several Type-K thermocouples implemented on the test apparatus.

4. Procedure and data analysis

The local heat transfer coefficient h and Nusselt number Nu are defined by Eqs. (1) and (2):

$$h = q_c^f/(T_w - T_{aw}) \tag{1}$$

$$Nu = hd/k_{air} \tag{2}$$

In Eq. (1) T_{aw} is the adiabatic wall temperature, q_c^f is the density heat flux evacuated from the plate front side by forced convection and k_{air} is the air thermal conductivity at the injection temperature. The typical range of temperature variation is 25 °C $< (T_w - T_j) <$ 65 °C with 17 °C $< T_j <$ 22 °C which leads to a film temperature value in between 30 and 40 °C. This weak variation allows us to evaluate the air thermal conductivity at the injection temperature.

The flows are controlled so that $T_j = T_{amb}$. Involved jet velocities are low enough to neglect any viscous heating effect. The distinction between total temperature and static temperature in the flow can be neglected as

well. Thermal conditions are such ($T_j = T_{amb}$ and overall flow heating due to the test plate circuits is low) that it is not necessary to take into account any recovery effect due to mixing and thermal entrainment which could have modified the fluid reference temperature along the plate. That is why the adiabatic wall temperature has been considered equal to the jet total temperature (Eq. (3)). Experimental validations have been carried out before any test run to confirm this assumption. The wall temperature T_w included in Eq. (1) corresponds to the front test plate temperature (Eq. (4)):

$$T_{aw} = T_j \tag{3}$$

$$T_w = T_f \tag{4}$$

The determination of local heat transfer coefficients h is based on the heated-thin-foil technique. It is directly linked to an heat flux balance on the plate front side which is submitted to the heat flux density q due to the electric heating. The procedure introduces radiation losses due to multi-reflexion between the impingement and injection plates (q_r^f) and radiation and convection losses (q_r^b, q_c^b) on the plate back side. For these last corrections, a back side overall coefficient h_b has been measured. It has been estimated that a uniform value for all the target plate was suitable ($h_b = 12\ \mathrm{Wm^{-2}\,K^{-1}}$, value corresponding to natural convection and radiative effect). Radial heat conduction within the impingement plate can be neglected and a monodimensional conduction calculation is adequate to link the temperature field of the impingement plate back side T_b to the front temperature field T_f. This was confirmed by a numerical analysis using the nodal method to model finely the conduction as it is in reality within the test plate, taking into account the heating circuit discretization, conduction within the copper circuits, the painting presence on the impingement plate, the image scanning and spatial integration process introduced by the infrared camera. Hence the four relationships Eqs. (5)–(8) express the heat flux balance which is represented in Fig. 4:

$$q_c^f = q - q_r^f - q_c^b - q_r^b \tag{5}$$

$$q_r^f = \sigma(1/\varepsilon_{inf} + 1/\varepsilon_f - 1)^{-1}\left(T_f^4 - T_{inj}^4\right) \tag{6}$$

$$q^b = q_c^b + q_r^b = h_b(T_b - T_{amb}) \tag{7}$$

$$T_f = T_b + (e/k_w)h_b(T_b - T_{amb}) \tag{8}$$

The expression of q_r^f takes the form of a correction by multi-reflexion between two infinite plates with uniform temperatures. This model of the radiation front exchanges was considered as sufficient in so far as the variation of temperature on the injection and impingement plates are small and q_r^f corresponds to a small amount of the total injected heat flux q (3–9%). The rear radiation and convection losses (q^b) are in the order of 9–12% of the total injected heat flux q in the impingement region. The local heat transfer coefficients and Nusselt number field on the entire impinged surface can finally be evaluated from Eqs. (1)–(8). The uncertainties due to the different parameters and measurements have been evaluated. In the impingement region the total relative error on the heat transfer coefficient is less than 10% and the random relative error (global error minus bias) is less than 5%. The uncertainty comes mainly from the uncertainty on the impingement plate back side emissivity and on the measurement of T_b.

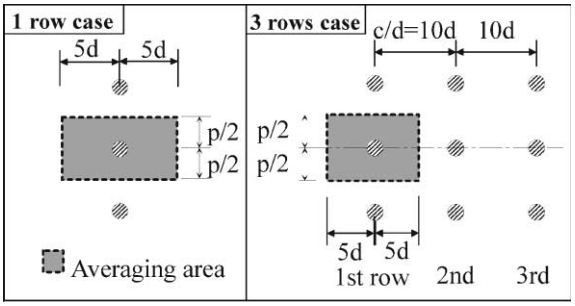

Fig. 5. Averaging area.

Only the test section centerline region (defined by the zone of influence of the three jets centered on the test section) is really used for data processing in order to eliminate any interference due to side effects. Averaging of local Nusselt numbers can then be introduced in order to analyse the parameters influence on the overall cooling efficiency. The averaging process is resumed by Eq. (9):

$$\bar{h} = \overline{q_c^f}/(\overline{T_w} - T_j) \tag{9}$$

The averaging area is the same in a one-row case and in a three-rows case (Fig. 5) independently of the impingement parameters so that the results can stand comparison in terms of overall cooling efficiency. It corresponds to the zone of influence of the middle jet of the upstream row. The area is limited in the spanwise direction by the zone of influence of the next jets. In the streamwise direction, experiments show that the impinging jet influence is of importance only $5d$ upstream and downstream of the jet which corresponds in the three-rows case to the influence limit of the second row.

5. Results and discussion

5.1. Geometry with several injection rows

Fig. 6 shows an example of the thermal footprints of three impinging jets obtained from the infrared measurements. Isotherms are perfectly axisymmetric except in the far field of the impingement. We do not notice

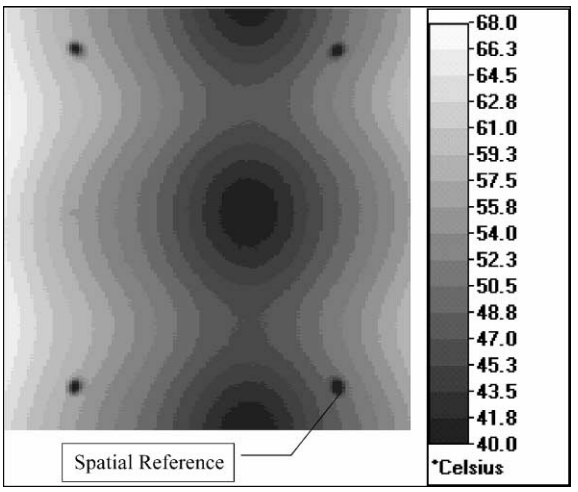

Fig. 6. An example of infrared measurement ($p/d = 4$, $Z/d = 5$, $Re = 10000$).

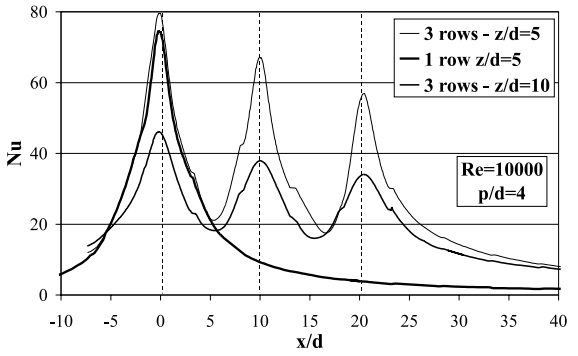

Fig. 7. Nusselt number streamwise profiles—comparison of a one-row case with a three-rows case.

sensitive influence of the fountain effect at the jets junction.

Detailed local Nusselt number distributions for a one-row case and two three-row cases are presented as functions of streamwise distance in Fig. 7. Profiles shown are centered on the jets. The dotted lines show the jet streamwise positions. Each impingement jet is responsible for a high heat transfer increase with a maximum reached at the stagnation point. The Nusselt number distributions of the one-row and three-row cases fit perfectly well within the zone of influence of the first row. Downstream of this region, heat transfer is drastically reduced in the one-row case since the impingement is not efficient anymore whereas the impinging jets of the two last rows maintain high heat exchanges in the three-rows configuration. The second and third rows have not any thermal effect on the first row. This was observed within the tested range of parameters even for the maximum impinging distance $Z/d = 10$ for which jet interaction between two rows is the most likely. The chosen streamwise spacing between two rows of the three-rows case ($c/d = 10$) is typical of a turbine geometry and is indeed large enough to reduce the streamwise jet interaction before impingement to a minimum level. The first row can then be analysed independently of the presence of downstream additional rows. The results will be representative of the behaviour of a single row of impinging jets and of the behaviour of the first row of an array of jets as well. One should notice that for an array of jets the air exhaust from the upstream jets disturbs the downstream impinging jets by creating a crossflow. Downstream jets are more or less deflected depending on the mass flow rate and the confinement involved (and thus on the impingement distance). Maximum and averaged heat transfer due to impingement are all the more reduced as spent air accumulates. These features are visible on the three-rows cases of Fig. 7: for $Z/d = 5$, stagnation point Nusselt number is reduced by 16% on the second row (17.4% for $Z/d = 10$) and by 28.7% on the third row (26.7% for $Z/d = 10$) when compared to the stagnation point Nusselt number on the first row. Furthermore one should notice the strong heat transfer decrease for high impingement distances. The Nusselt number values decrease around 42–43% for the first two stagnation points ($x/d = 0$ and 10) and around 32% for the third stagnation point ($x/d = 20$) between the $Z/d = 5$ case and the $Z/d = 10$ case. The results that will be presented concerned only one row. They should then be modulated if application to downstream jets of an array is looked at.

5.2. Influence of the Reynolds number

Five impingement Reynolds numbers have been tested: $Re = 3000$, 7000, 10 000, 15 000 and 20 000. The streamwise and spanwise distributions of local Nusselt numbers for $p/d = 4$ and $Z/d = 2$ are shown in Fig. 8. These profiles are centered on the jet. For $Re = 3000$, the impingement is very weak and heat transfer is low. Local heat transfer is a growing function of Re. Fig. 9 presents the minimum and maximum values of local Nu extracted from the spanwise profile as a function of Re. The maximum value corresponds to the stagnation point heat transfer whereas the minimum Nu is found for $y = p/2$. The fountain effect does not seem to have a sensitive effect on the wall exchange. The Nusselt number value at $p/d = \pm 2$ (in the middle of two jets, where this effect is the more important) is sensibly the same the one obtained in the x-direction ($x/d = 2$). The averaged Nusselt number calculated over the surface defined in Fig. 5 is plotted in Fig. 9 as well. The variation of the averaged Nusselt number can be approximated by a power-law dependence based on $Re^{0.88}$.

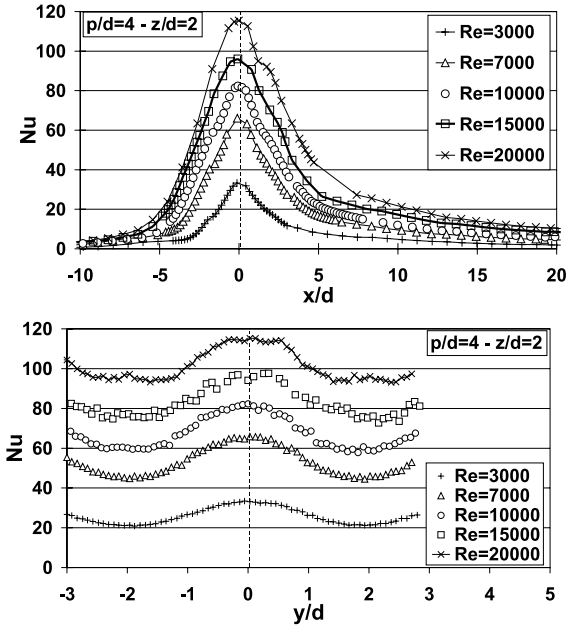

Fig. 8. Streamwise and spanwise distributions of Nusselt numbers in a one-row configuration for different injection Reynolds numbers.

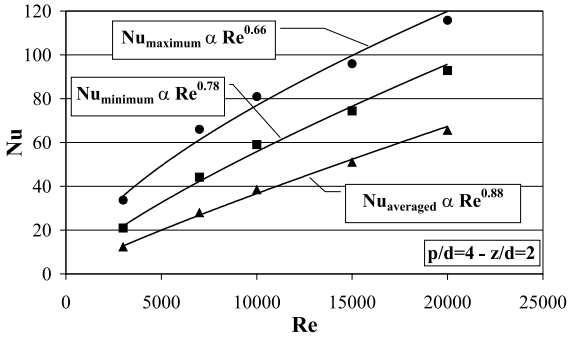

Fig. 9. Variation of minimum, maximum and averaged Nusselt numbers with the injection Reynolds number.

5.3. Influence of impingement distance z

Heat transfer variations with the impingement distance Z/d have been investigated extensively. A few spanwise Nusselt profiles extracted from these measurements are displayed in Fig. 10. The impingement distance $Z/d = 2$ leads to the highest local heat transfer over the range of impingement distances tested. Fig. 10 illustrates this result which is in accordance with the results of Baughn and Shimizu [21] who pointed out the same impingement distance for a single impinging jet. Nevertheless Fig. 10 shows as well that the heat transfer rate generated by the impingement distance $Z/d = 5$ is very closed to the heat transfer rate for $Z/d = 2$. All

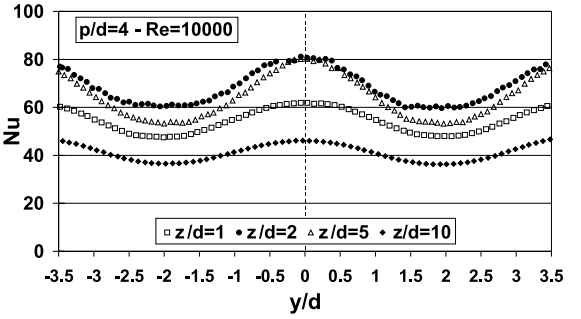

Fig. 10. Spanwise distributions of Nusselt numbers in a one-row configuration for different impingement distances.

these results are independent of the injection Reynolds number and the spacing p/d. As a consequence, the maximum averaged Nusselt number is obtained for $Z/d = 2$ within the range of distances tested. The continuous variations of the averaged Nusselt number as a function of the impingement distance have been interpolated from the measurements for different spacings p/d (Fig. 11). Then for a given spanwise jet spacing, an optimum impingement distance Z/d have been identified. Fig. 11 shows that a value of Z/d close to 3 seems indeed to correspond to a maximum averaged heat transfer, independently of p/d. Nevertheless the differences for distances $2 < Z/d < 4$ are quite low. This is partly due to the fact that the surface over which the Nusselt numbers are averaged is quite large in the streamwise direction which tends to smooth the results. Heat transfer rate rapidly decreases for impingement distance below $Z/d = 2$. At these distances, the confinement effect is greatly penalizing and one should a priori avoid these values to improve the cooling efficiency. Heat transfer rate decreases as well when the impingement distance increases beyond $Z/d = 5$. At $Z/d = 10$, the impingement is too weak to cool efficiently the surface. As a rule of thumb, it would therefore be a good design practice to choose for a first attempt an impingement distance $Z/d = 3$.

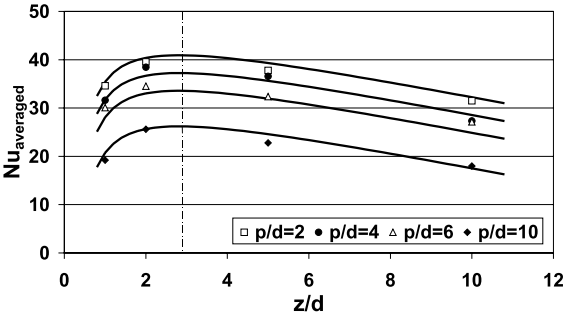

Fig. 11. Variation of the averaged Nusselt number with the impingement distance for different spanwise spacings.

5.4. Optimization of geometry and of injection rate

The quantity of air used to cool is connected to the number of injections and to the injected flow rate of each orifice.

In Fig. 11, one should not compare directly averaged Nusselt numbers for different spanwise spacings p/d. Indeed the value p/d governs directly the surface over which the averaged Nusselt number is calculated (Fig. 5). As an example averaged Nusselt numbers for $p/d = 2$ are higher than for $p/d = 4$ (Fig. 11) but it does not mean the cooling is more efficient for $p/d = 2$ since the surface cooled taken into account is larger for $p/d = 4$ than for $p/d = 2$. The same consideration is of importance when looking at Fig. 12. For a given impingement distance the averaged Nusselt number is a decreasing function of p/d but this function originates from the process of averaging and is not representative of a cooling weakening. Fig. 12 should then only be analysed vertically: at a given value of p/d, one can again notice the relative influence of the impingement distance.

To evaluate the overall cooling efficiency of the different impingement configurations and to be able to compare the different impingement cases, one can work at a fixed mass flow rate of coolant per unit area of cooled surface G_s [22]. G_s represents the air quantity devoted to the cooling of a given surface: the aim of the designer is then to obtain maximum heat transfer rates minimizing G_s. In our study G_s is expressed by Eq. (10).

$$G_s = \rho V_j (\pi d^2/4)/(p \times 10d)^{-1} \tag{10}$$

At a given impingement distance, averaged Nusselt numbers are expressed as a function of G_s in Figs. 13–16. A network of Nusselt number curves depending on p/d and Re is derived from the measurements and plotted for each value of Z/d. Increasing the injection Reynolds number at a fixed value of p/d or decreasing the spanwise spacing p/d at a fixed value of Re increase heat transfer rates. Nevertheless it means that G_s is increased

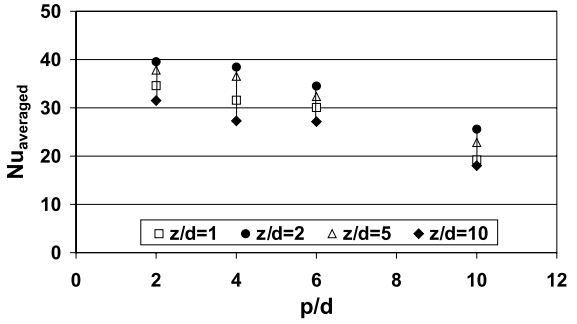

Fig. 12. Variation of the averaged Nusselt number with the spanwise spacing for different impingement distances.

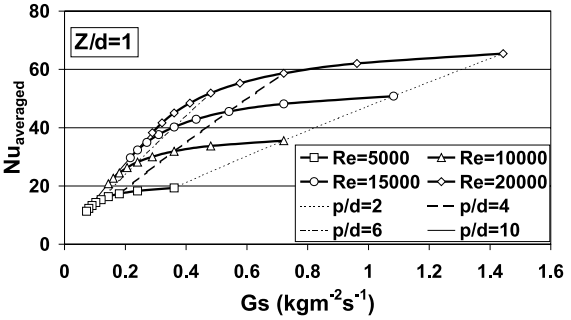

Fig. 13. $Nu = f(G_s)$ $Z/d = 1$.

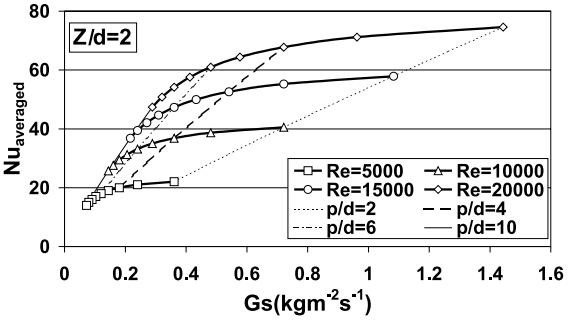

Fig. 14. $Nu = f(G_s)$ $Z/d = 2$.

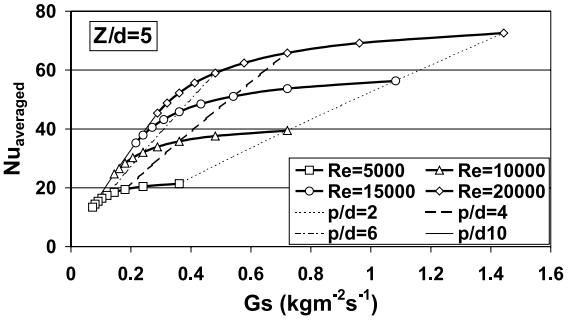

Fig. 15. $Nu = f(G_s)$ $Z/d = 5$.

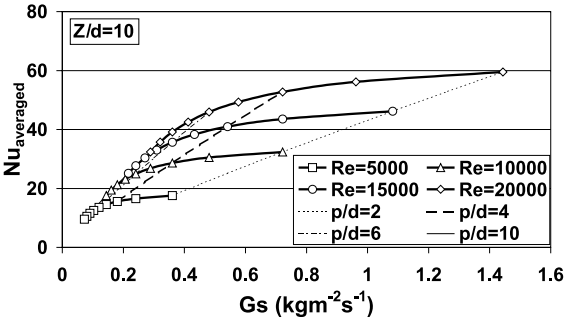

Fig. 16. $Nu = f(G_s)$ $Z/d = 10$.

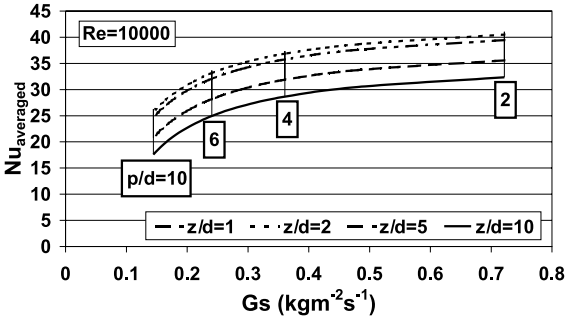

Fig. 17. $Nu = f(G_s)$—inluence of Z/d.

as well. For a fixed value of G_s, the overall cooling efficiency is proportional to the averaged Nusselt number. Figs. 13–16 show that for a fixed value of G_s, independently of the impingement distance (Z/d), the designer interest is to increase the injection Reynolds number and increase p/d as well rather than the contrary. In this way heat transfer rates are increased and the mass flow rate of cooling air is kept constant. As an example, for $Z/d = 2$ or 5 (Figs. 14 and 15) and G_s fixed at 0.72, heat transfer is increased by 70% when changing the impingement configuration from $p/d = 2$ and $Re = 10\,000$ to $p/d = 4$ and $Re = 20\,000$. Furthermore Figs. 13–16 point out that for a given impingement distance and a given Reynolds number, it is not efficient to increase the mass flow rate of coolant per unit area of cooled surface G_s by decreasing p/d beyond a certain point. Thus, for $Z/d = 5$, $Re = 10\,000$ or $20\,000$, heat transfer is increased by 45% when p/d changes from 10 to 4 (G_s is then increased by 250%) and only by 10% when p/d changes from 4 to 2 (G_s increased again by 200%). Over the range of impingement distances and Reynolds numbers tested, it seems there is no point in decreasing the spanwise spacing below $p/d = 4$–5: beyond this point, heat transfer improvement does not balanced the cost due to the large increase in the amount of air required. This result is visible in Fig. 17 as well as the influence of the impingement distance Z/d. Again $Z/d = 2$ appears as the most efficient distance among the distances tested in this study.

6. Conclusion

Local and averaged heat transfer coefficients were measured using the heated-thin-foil technique associated with infrared measurements for a row of confined jets impinging on a flat plate. Spent air was constrained to exit in a single direction to be representative of a turbine internal cooling system. The influences of the impingement distance, the injection Reynolds number and the spanwise spacing between jets were investigated. The mass flow rate of coolant per unit area of cooled surface G_s was introduced to compare the results in terms of overall cooling efficiency. It is indeed the first parameter the designer have to minimize to optimize the cooling system if he takes only into account the heat transfer rates and not the temperature uniformity of the cooled surface. The measurements pointed out an optimum impingement distance (maximum heat transfer rates) within the range $Z/d = 2$ and $Z/d = 5$. A value of $Z = 3d$ could be a good design practice. Increasing Re and decreasing p/d tend to improve heat transfer rates. At a fixed value G_s, it is more interesting to increase Re and p/d than decreasing p/d. An optimum spanwise spacing $p/d = 4$–5 was identified. Within the range of our study, it is not worth taking a lower value for p/d as the cost in terms of amount of cooling air required is too high compared to the heat transfer enhancement. Again this does not take into account any temperature uniformity criteria.

Acknowledgements

The authors wish to thank *SNECMA Moteurs* for their involvement and support during this investigation.

References

[1] C. Son, D. Gillespie, P. Ireland, G.M. Dailey, Heat transfer and flow characteristics of an engine representative impingement cooling system, Proceedings of ASME Turboexpo, Munich, Germany, May 8–11, 2000.
[2] H. Martin, Heat and mass transfer between impinging gas jets and solid surfaces, Advances in Heat Transfer 13 (1977) 1–60.
[3] S.J. Downs, E.H. James, Jet impingement heat transfer—A literature survey, ASME paper no. 87-HT-35, The National Heat Transfer Conference, Pittsburgh, Pennsylvania, 1987.
[4] K. Jambunathan, E. Lai, M.A. Moss, B.L. Button, A review of heat transfer data for single circular jet impingement, Int. J. Heat Fluid Flow 13 (2) (1992) 106–115.
[5] R. Viskanta, Heat transfer to impinging isothermal gas and flame jets, Experimental Thermal and Fluid Science 6 (1993) 111–134.
[6] A.I. Behbahani, R.J. Goldstein, Local heat transfer to staggered arrays of impinging circular air jets, Journal of Engineering for Power 105 (1983) 354–360.
[7] B.R. Hollworth, G.H. Cole, Heat transfer to arrays of impinging jets in a crossflow, Journal of Turbomachinery 109 (1987) 564–571.
[8] K.W. Van Treuren, Z. Wang, P.T. Ireland, T.V. Jones, Detailed measurements of local heat transfer coefficient and adiabatic wall temperature beneath an array of impinging jets, Journal of Turbomachinery 116 (1994) 369–374.
[9] K.W. Van Treuren, Z. Wang, P.T. Ireland, T.V. Jones, S.T. Kohler, Comparison and prediction of local and average

heat transfer coefficients under an array of inline and staggered impinging jets, ASME 96-GT-163, Birmingham, 1996.

[10] K.R. Saripalli, Visualization of multijet impingement flow, AIAA Journal 21 (4) (1983) 483–484.

[11] J.A. Parsons, J.C. Han, Rotation effect on jet impingement heat transfer in smooth rectangular channels with heated target walls and radially outward cross flow, International Journal of Heat and Mass Transfer 41 (13) (1998) 2059–2071.

[12] L.W. Florschuetz, C.R. Truman, D.E. Metzger, Streamwise flow and heat transfer distributions for jet array impingement with crossflow, Journal of Heat Transfer 103 (1981) 337–342.

[13] L.W. Florschuetz, R.A. Berry, D.E. Metzger, Periodic streamwise variations of heat transfer coefficients for inline and staggered arrays of circular jets with crossflow of spent air, Journal of Heat Transfer 102 (1980) 132–137.

[14] L.W. Florschuetz, Y. Isoda, Flow distribution and discharge coefficient effects for jet array impingement with initial crossflow, Journal of Engineering for Power 105 (1983) 296–304.

[15] L.W. Florschuetz, D.E. Metzger, C.C. Su, Heat transfer characteristics for jet array impingement with initial crossflow, Journal of Heat Transfer 106 (1984) 34–41.

[16] D.E. Metzger, L.W. Florschuetz, D.I. Takeuchi, R.D. Behee, R.A. Berry, Heat transfer characteristics for inline and staggered arrays of circular jets with crossflow of spent air, Journal of Heat Transfer 101 (1979) 526–531.

[17] P. Brevet, E. Dorignac, J.J. Vullierme, Mach number effect on jet impingement heat transfer, heat transfer in gas turbine systems, Annals of the New York Academy of Sciences 934 (2001) 409–416.

[21] J.W. Baughn, S. Shimizu, Heat transfer measurements from a surface with uniform heat flux impinging jet, Journal of Heat Transfer 111 (1989) 1096–1098.

[22] R.J. Goldstein, W.S. Seol, Heat transfer to a row of impinging circular air jets including the effect of entrainment, International Journal of Heat and Mass Transfer 34 (8) (1991) 2133–2146.